Organic Spin Ladders from Tetrathiafulvalene (TTF) Derivatives**

By *Xavi Ribas*, *Marta Mas-Torrent*, *Aarón Pérez-Benítez*, *Joao C. Dias*, *Helena Alves*, *Elsa B. Lopes*, *Rui T. Henriques*, *Elies Molins*, *Isabel C. Santos*, *Klaus Wurst*, *Pascale Foury-Leylekian*, *Manuel Almeida*,* *Jaume Veciana*, and *Concepció Rovira**

Starting from the first organic spin ladder reported, a dithiophene-tetrathiafulvalene salt ((DT-TTF)$_2$[Au(mnt)$_2$]) (mnt = maleonitriledithiolate), two different approaches to enlarge the family of organic spin-ladder systems are described. The first approach consists of a molecular variation of the donor; to that purpose, the new TTF derivative ethylenethiothiophene-tetrathiafulvalene (ETT-TTF, **3**), is synthesized and structurally characterized. From this donor a new ladder-like structure compound, (ETT-TTF)$_2$[Au(mnt)$_2$] (**4**), isostructural with (DT-TTF)$_2$[Au(mnt)$_2$], is obtained. However, the magnetic properties of **4** do not follow the known spin-ladder behavior owing to orientational disorder exhibited by the ETT-TTF molecules in the crystal structure. In the second approach, the acceptor complex is changed, either in the nature of the ligand or in the metal. With the [Au(i-mnt)$_2$]$^-$ salt (i-mnt = iso-maleonitriledithiolate), the new ladder-like compound (DT-TTF)$_2$[Au(i-mnt)$_2$] (**5**), isostructural with **4**, is obtained, but only as a minority product. Two other compounds with a different anion generated in situ, bearing a Au(I) dimeric core, were also isolated; (DT-TTF)$_9$[Au$_2$(i-mnt)$_2$]$_2$ (**6**) as the most abundant phase and (DT-TTF)$_2$[Au$_2$(i-mnt)$_2$] (**7**) as another minority phase. Salt **7** is characterized by X-ray crystallography as a chiral compound, due to the torsion of the ligands around the central Au–Au bond. The magnetic properties of (DT-TTF)$_2$[Au(i-mnt)$_2$] (**5**) indicate that it follows a spin-ladder behavior and the electron paramagnetic resonance (EPR) data is fitted to the Troyer and Barnes and Riera equations with the parameters $\Delta/k_B = 71$ K, $J_{\parallel}/k_B = 86$ K, and $J_{\perp}/k_B = 142$ K, indicating a $J_{\perp}/J_{\parallel}$ ratio of 1.65. The change of the gold complex [Au(mnt)$_2$] for its copper analogue, [Cu(mnt)$_2$] also leads to a ladder-like structure, (DT-TTF)$_2$[Cu(mnt)$_2$] (**8**), which is isostructural with the gold analogue and with salts **4** and **5.** The fully ionic salt (DT-TTF)[Cu(mnt)$_2$] (**9**) is also obtained. The magnetic properties demonstrated that compound **8** is the third organic spin-ladder system of this family, and the values found by a fitting to the ladder equations were $\Delta/k_B = 123$ K, $J_{\parallel}/k_B = 121$ K, and $J_{\perp}/k_B = 218$ K, corresponding to a $J_{\perp}/J_{\parallel}$ ratio of 1.75, similar to that of **5** and close to that of an ideal spin ladder.

[*] Prof. M. Almeida, J. C. Dias, Dr. H. Alves, Dr. E. B. Lopes, Dr. I. C. Santos
Departamento de Química, Instituto Tecnológico e Nuclear/Centro de Física da Matéria Condensada da Universidade de Lisboa
P-2686-953 Sacavém (Portugal)
E-mail: malmeida@itn.pt

Prof. C. Rovira, Dr. X. Ribas, Dr. M. Mas-Torrent, A. Pérez-Benítez, Prof. E. Molins, Prof. J. Veciana
Institut de Ciència de Materials de Barcelona, CSIC
Campus de la UAB, E-08193 Bellaterra (Spain)
E-mail: cun@icmab.es

Prof. R. T. Henriques
Instituto de Telecommunicações, Polo de Lisboa
Instituto Superior Técnico, P-1049-001 Lisboa (Portugal)

Dr. K. Wurst
Institut für Allgemeine Anorganische und Theoretische Chemie
Universität Innsbruck, Innrain 52a, A-6020 Innsbruck (Austria)

Prof. P. Foury-Leylekian
Laboratoire de Physique des Solides
Bâtiment 510, Univ. Paris-Sud, F-91405 Orsay (France)

[**] This work was supported in Spain by DGI project BQU2003-00760, and by DGR Catalonia, project 2001SGR00362, and in Portugal by FCT under contract POCTI/35342/QUI/2000. The collaboration between authors in Barcelona and Sacavém was supported by the ICCT-CSIC bilateral agreement, and additional support was provided through COST D14. Supporting Information is available from the authors or on Wiley InterScience (www.wileyinterscience.com). X-ray crystallographic files for ETT-TTF (**3**), (ETT-TTF)$_2$[Au(mnt)$_2$] (**4**), (DT-TTF)$_2$[Au(i-mnt)$_2$] (**5**), (DT-TTF)$_2$[Au$_2$-(i-mnt)$_2$]$_2$ (**7**), (DT-TTF)$_2$[Cu(mnt)$_2$] (**8**), and (DT-TTF)[Cu(mnt)$_2$] (**9**) (CIF). ORTEP plots for compounds **4**, **5**, **7**, **8**, and **9**. Crystal packing data for compounds **5** and **8**. EPR intensity versus *T* plot for compounds **4** and **9**. Picture of diffuse X-ray measurement at 200 K for **8**.

1. Introduction

Spin ladders are a class of low-dimensional magnetic systems that consist of a finite number of strongly magnetically coupled chains of spins that are intermediate between those of one-dimensional (1D) chains and two-dimensional (2D) planes (Fig. 1). These systems are particularly interesting as a result of the increased importance of the quantum-mechanical effects operating within them. Theoretical calculations have predicted that spin ladders with an odd number of legs behave as chains with a finite susceptibility upon approaching zero temperature, whereas those with an even number of legs have a gap in the magnetic excitations and the susceptibility drops exponentially towards zero upon cooling, but with a spin-liquid ground state, so called because of the purely short-range spin correlation along the legs. In fact these even-legged ladders consist of spin-singlet pairs with a spin–spin correlation distance along the legs that shows an exponential decay produced by the presence of a finite spin gap.[1]

In most spin-ladder examples, the spins are located in transition metals either in inorganic oxides,[2] or copper(II) halides.[3] Nevertheless, molecular spin ladders have also emerged from the initiation of this area of research.[4,5] By using planar molecules as spin-carrier units, the interacting spins are located in molecular orbitals which can be entirely of π nature. The existing examples of molecular spin ladders clearly show that typ-

 DOI: 10.1002/adfm.200400407

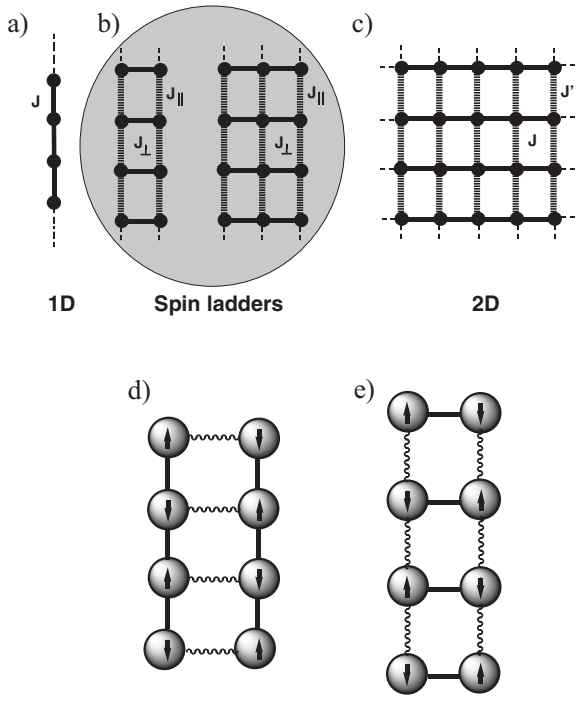

Figure 1. Schematic representation of different kinds of low-dimensional magnetic Heisenberg systems with antiferromagnetic couplings: a) 1D chain; b) Two-legged and three-legged spin ladders where $J_{\perp}$ is the coupling along the rungs and $J_{\|}$ is the coupling along the chains; c) 2D square lattice with different exchange coupling constants, J and J'. Black dots denote $S = 1/2$ spin-containing units and continuous and dashed lines represent antiferromagnetic interactions of different strength. Construction of molecular two-legged ladders by d) the assembly of 1D $S = 1/2$ chains, and e) connection of $S = 1/2$ dimers.

ical supramolecular- and crystal-engineering criteria, such as π–π overlap, S···S and C–H···S interactions, and complementarity of size and shape, are useful in the construction of these magnetic quantum systems with dimensionalities intermediate between 1D chains and 2D square lattices.[5]

The construction of the simplest molecular spin ladder–a two-legged ladder—can be conceptually achieved following two different strategies: the first one, (Fig. 1d) by the connection of two molecular 1D $S = 1/2$ spin chains, one next to the other, and the second (Fig. 1e), by assembling an infinite number of units with two interacting $S = 1/2$ molecules (dimers).

We have followed the first strategy—the assembling of chains—to construct spin ladders by using as building block a tetrathiafulvalene (TTF) derivative, dithiophene-tetrathiafulvalene (DT-TTF), which crystallizes in stacks forming 1D chains that are connected by S···S interactions (Fig. 2).[6] A two-legged spin ladder was obtained in the salt (DT-TTF)$_2$[Au(mnt)$_2$],[4a,b] with a crystal structure consisting of pairs of interacting charged donor stacks, with the same arrangement as in the neutral compound, that are separated by stacks of the diamagnetic monoanion Au(mnt)$_2^-$ (mnt = maleonitriledithiolate). This planar diamagnetic counter-ion has the same size as the donor and also exhibits a great tendency to stack, forming 1D chains, therefore being complementary to DT-TTF.

The spin-carrying units of the ladder are dimers of DT-TTF, that are formed below 220 K; these contain one electron and the antiferromagnetic exchange strengths are $J_{\text{rail}}\,(J_{\|}) = 82$ K and $J_{\text{rung}}\,(J_{\perp}) = 142$ K. Recent infrared (IR) variable-temperature studies of this system show that there is a transition at 70 K associated with both vibrational and magnetic properties in the rail direction.[7] Clearly, additional similar systems are necessary to shed light on the mechanisms giving rise to all these properties, and of special interest will be those with the same structure and similar components but having some differences in the strength of the magnetic interactions along the rails and along the rungs, that is, $J_{\|}$ and $J_{\perp}$ parameters.

A priori, there are two possible ways to achieve this goal: a) to exchange the DT-TTF derivative for a donor having similar structural and electronic characteristics, and b) to exchange the [Au(mnt)$_2$]$^-$ counter-ion with an analogous one that can maintain the size and shape complementarities with the donor.

In this paper we describe the results achieved following both strategies; the results demonstrate how subtle the interplay of factors leading to the spin-ladder magnetic properties is.

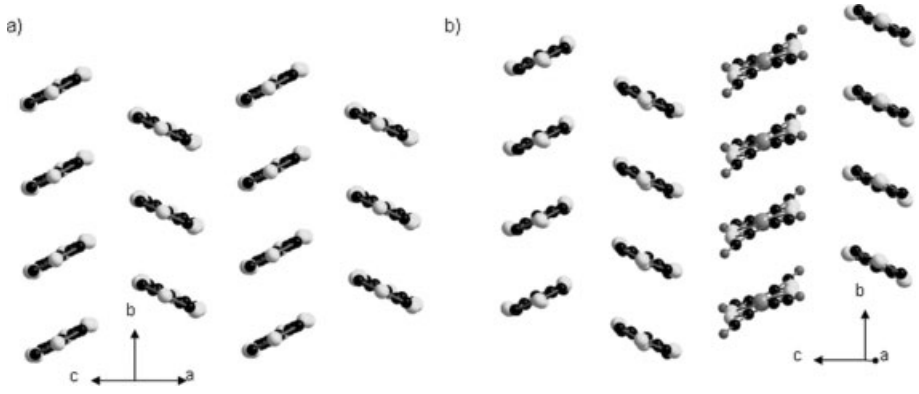

Figure 2. View of the crystal packing of a) DT-TTF and b) (DT-TTF)$_2$[Au(mnt)$_2$] [4a]. Hydrogen atoms have been omitted for clarity.

ADVANCED FUNCTIONAL MATERIALS

2. Results and Discussion

2.1. First Approach: Combination of the Same Gold Complex, $[Au(mnt)_2]^-$, with a New Thiophene-TTF Donor

We choose as a donor target the dissymmetric molecule ethylenethiothiophene-tetrathiafulvalene (ETT-TTF), in which one of the thiophene rings of DT-TTF is replaced by a dihydrothiophene ring with the sulfur atom in a position able to promote more lateral S···S interactions between the donor stacks (Scheme 1), which could derive in stronger magnetic interactions in the rungs of the ladder ($J_\perp$).

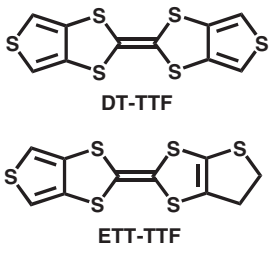

Scheme 1. Structures of OT-TTF and ETT-TTF.

ETT-TTF was obtained by the cross-coupling of the suitable thione and ketone in neat boiling trimethyl phosphite, as shown in Scheme 2. The coupling of 4,5-ethylenethio-1,3-dithiol-2-one (**1**)[8] and thiophene-1,3-dithiol-2-thione (**2**)[6,9] in a 1:1 proportion gave rise to a mixture of the desired donor, ETT-TTF (**3**), and the symmetrical byproducts bis(ethylenethio)tetrathiafulvalene (BET-TTF) and DT-TTF, which were separated by column chromatography. Owing to the formation of these symmetric derivatives, the yield of ETT-TTF (**3**) was low (24 %). By varying the ketone **1**/thione **2** proportion to 1:2, only DT-TTF and the dissymmetric ETT-TTF donors were obtained, resulting in an easier purification of the compounds. Nevertheless, the yield of the desired compound was lower, 15 %, due to a worse coupling yield.

Needle-shaped single crystals of ETT-TTF suitable for X-ray analysis were obtained by recrystallization in CH_2Cl_2. The crystallographic parameters are given in Table 1 and the molecular structure and the corresponding atomic numbering are shown in Figure 3. ETT-TTF crystallizes in the monoclinic centrosymmetrical *C*2/*c* space group and the asymmetric unit contains half a molecule. This fact means that there is 50 % disorder in the position of the TTF substituents along the long axis of the molecule; that is 50 % of the molecules present the aromatic ring in one position and 50 % the dihydrothiophene ring. In addition, as is the case in the BET-TTF donor[6] and most of its radical-ion-salt derivatives, there is a positional disorder in the sulfur atom of the dihydrothiophene ring being statistically distributed over the two available positions (occu-

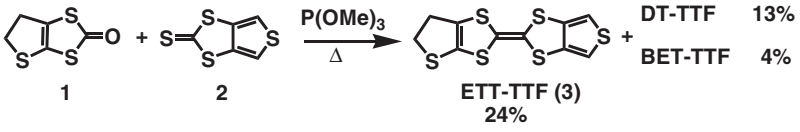

Scheme 2. Synthetic route to ETT-TTF.

Table 1. Crystallographic data of the new compounds reported.

Compound	ETT-TTF (**3**)	$(ETT\text{-}TTF)_2$ $[Au(mnt)_2]$ (**4**)	$(DT\text{-}TTF)_2$ $[Au(i\text{-}mnt)_2]$ (**5**)	$(DT\text{-}TTF)_2$ $[Au_2(i\text{-}mnt)_2]$ (**7**)	$(DT\text{-}TTF)_2$ $[Cu(mnt)_2]$ (**8**)	(DT-TTF) $[Cu(mnt)_2]$ (**9**)
Formula	$C_{10}H_6S_6$	$C_{28}H_{12}AuN_4S_{16}$	$C_{28}H_8AuN_4S_{16}$	$C_{28}H_8Au_2N_4S_{16}$	$C_{28}H_8CuN_4S_{16}$	$C_{18}H_4CuN_4S_{10}$
Molecular mass	318.5	1114.34	1110.31	1307.28	976.88	660.39
T [K]	293(2)	293(2)	223(2)	224(2)	293(2)	293(2)
Dimensions [mm]	0.57 × 0.11 × 0.10	0.4 × 0.1 × 0.05	0.5 × 0.04 × 0.01	0.1 × 0.05 × 0.01	0.7 × 0.2 × 0.03	0.6 × 0.14 × 0.1
Crystal color	yellow	brown	dark blue	black	black	black
Crystal system	monoclinic	monoclinic	monoclinic	tetragonal	monoclinic	monoclinic
Space group	C2/c	$P2_1/n$	$P2_1/n$	$P4_32_12$	$P2_1/n$	$P2_1/c$
a [Å]	26.236(2)	16.437(4)	16.494(3)	8.318(2)	16.2990(5)	3.7990(7)
b [Å]	4.017(1)	3.9800(10)	3.8670(8)	8.318(2)	3.9079(3)	12.4540(16)
c [Å]	11.140(1)	27.110(13)	27.161(5)	50.760(6)	27.3225(17)	24.473(2)
α [°]	90	90	90	90	90.000(5)	90.000(5)
β [°]	91.136(7)	101.31(4)	99.52(3)	90	102.141(5)	93.587(14)
γ [°]	90	90	90	90	90.000(5)	90.000(5)
Volume [Å^3]	1173.8(3)	1739.1(10)	1708.6(6)	3512.0(13)	1701(2)	1155.6(3)
Z	4	2	2	4	2	2
ρ_{calc} [g cm^{-3}]	1.79	2.128	2.158	2.472	1.907	1.898
Intervals *h*, *k*, *l*	0–36, 0–5, ± 15	± 19, 0 + 15, 0 + 32	0 + 15, ± 3, –26 + 25	± 7, ± 7, ± 48	0 + 19, 0–4, –31 + 32	0–4, 0–14, ± 29
$2\theta_{max}$ [°]	60.7	49.90	40.12	42	66.90	50.00 deg
Reflections collected	1782	3140	4674	3705	3126	2325
Indep. reflections	1782	3072	1603	1342	3012	2006
Reflections > 2σ (I)	1268	2050	1292	1044	1868	913
*R*1	0.0678	0.0530	0.0287	0.0495	0.0522	0.0701
*wR*2	0.1767	0.1337	0.0516	0.0909	0.0982	0.0911

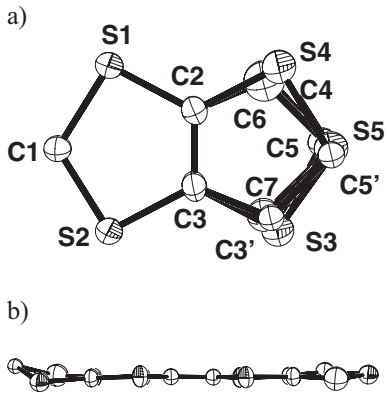

Figure 3. a) ORTEP [10] view of the asymmetric unit of ETT-TTF (**3**). Hydrogen atoms have been omitted for clarity. b) View of one ETT-TTF molecule parallel to the TTF core.

pancy factor of 0.5). This disorder does not affect the TTF core.

As it can be seen in Figure 3b, the ETT-TTF molecule deviates from planarity, since, whereas the thiophene ring is nearly planar, the non-aromatic substituent forms an angle of 10.28° or 7.75° (50 % disorder) with respect to the mean molecular plane owing to the folding of the ethylene group.

The ETT-TTF molecules are packed in the crystal-forming regular stacks along the crystallographic *b*-axis (Fig. 4) in a herringbone pattern. The molecules in adjacent stacks form opposite angles of 63.8° and –67.8° with respect to the stacking axis. The packing of the ETT-TTF donor is almost identical to that of DT-TTF.[6] The distance between the mean molecular planes of two consecutive ETT-TTF molecules inside the stacks is 3.661 Å, slightly larger than that found in the structure of DT-TTF (3.547 Å), with the molecular overlapping (Fig. 4c) almost identical. There are short (≤4 Å) S···S contacts between molecules of different stacks through the lateral S atoms. As predicted, since ETT-TTF has one more lateral S atom, there are more S···S short contacts, as depicted by dashed lines in Figure 4a.

The redox properties of the new donor ETT-TTF (**3**) were studied in dimethylformamide (DMF) solution by cyclic voltammetry with tetrabutylammonium hexafluorophosphate as the supporting electrolyte. As expected, this donor exhibited two reversible one-electron redox waves at 0.64 V and 0.85 V (in DMF, vs. Ag/AgCl), which indicates that it forms a stable cation radical and a stable dication. The cation-radical stability was also established by electron paramagnetic resonance (EPR) spectroscopy in solution, since the three-line signal, arising from the coupling with the two methylene protons in the α position ($a_H = 4.1$ G), remained unchanged for several days. ETT-TTF shows better donor properties than DT-TTF because the value of $E^1_{1/2}$ for ETT-TTF (0.64 V) is lower than for DT-TTF (0.78 V).

The similarities of both the electronic and structural properties of DT-TTF and ETT-TTF (**3**) donors make this new π-electron donor very promising for the purpose of preparing spin-ladder compounds by combination with the $[Au(mnt)_2]^-$ anion.

Indeed, by electrocrystallization of the donor ETT-TTF with the tetrabutylammonium salt of the bis(maleonitriledithiolate) Au(III) complex in CH_2Cl_2 over platinum electrodes, dark single crystals of the mixed-valence salt $(ETT\text{-}TTF)_2[Au(mnt)_2]$ (**4**) were obtained.

Salt **4** crystallizes in the monoclinic space group $P2_1/n$, being isostructural with the $(DT\text{-}TTF)_2[Au(mnt)_2]$ salt.[4a,b] The crystal and refinement data are given in Table 1. The asymmetric unit of the cell contains one ETT-TTF donor and half of the $Au(mnt)_2$ molecule, both moieties being almost planar (see structural description in Supporting Information). ETT-TTF molecules in the crystal are disordered, with 50 % of molecules being in one position, and 50 % in the position resulting from a rotation of 180° around the central C=C bond.

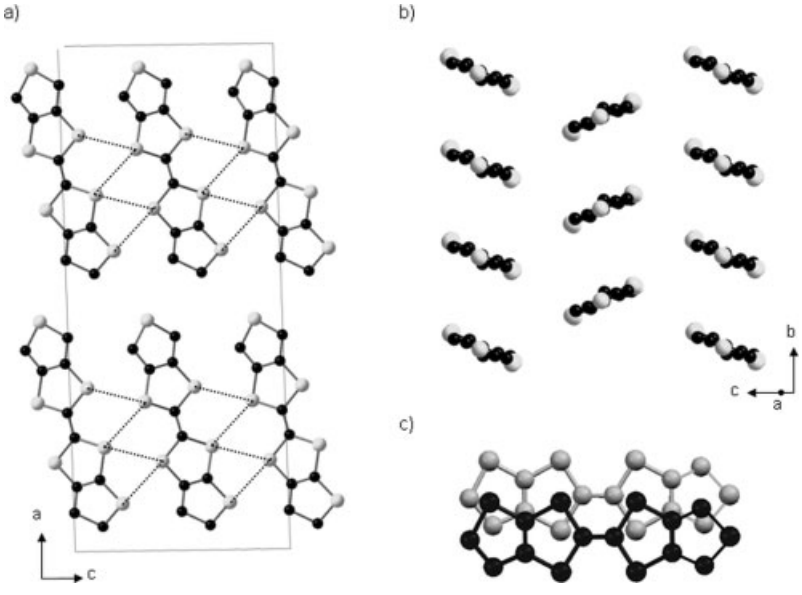

Figure 4. Projection of the crystal structure of ETT-TTF (**3**). For purposes of clarity only one of the possible molecules has been drawn. a) View along the stacking axis *b* (dashed lines show S···S contacts shorter than 4 Å), b) view parallel to the long molecular axes, and c) overlap of two consecutive molecules within a stack.

Molecules of both ETT-TTF and $[Au(mnt)_2]$ form tilted stacks along *b*-axis in a herringbone pattern. The ETT-TTF stacks are arranged in pairs related by a two-fold screw axis parallel to the *b*-axis (Fig. 5). Pairs of ETT-TTF stacks, in which molecules have an interplanar distance of 3.584 Å, alternate in the *a*,*c*-plane with isolated columns of $[Au(mnt)_2]$. Pairs of donor stacks are strongly connected through five short S···S contacts that are in the range between 3.574 and 3.728 Å, forming, in that way, a structural ladder. ETT-TTF molecules are in turn connected to $Au(mnt)_2$ by three short S···S contacts in the range between 3.623 and 3.786 Å (Fig. 5a and Table S1 in the Supporting Information).

As in the case of the $(DT\text{-}TTF)_2[Au(mnt)_2]$ salt, the crystal structure of $(ETT\text{-}TTF)_2[Au(mnt)_2]$ (**4**) is very similar to that of the donor component, the ETT-TTF (**3**), and can be

ADVANCED FUNCTIONAL MATERIALS

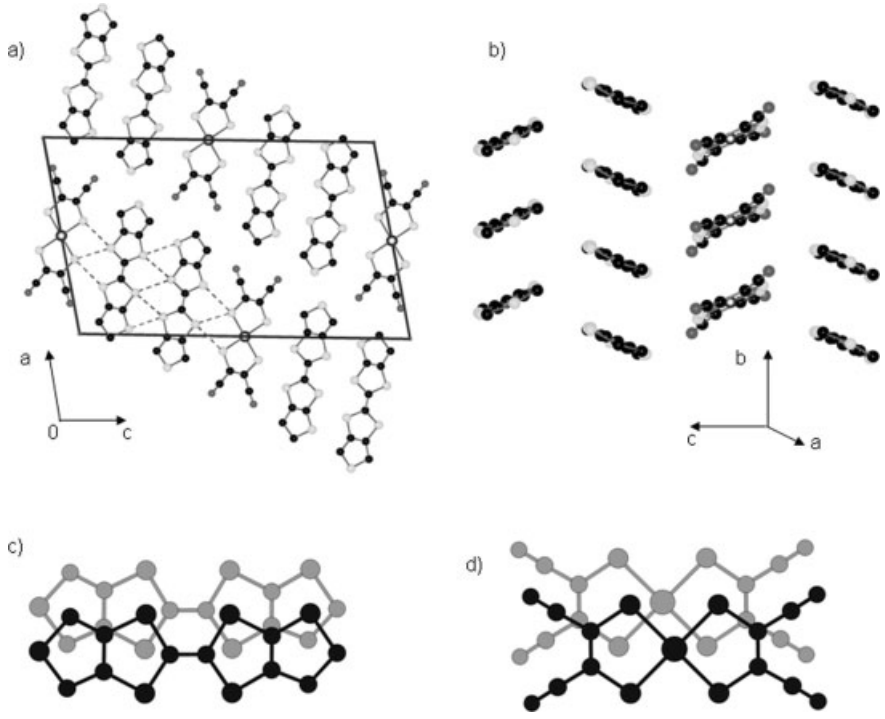

Figure 5. Projection of the crystal structure of (ETT-TTF)$_2$[Au(mnt)$_2$] (**4**); for purposes of clarity only one of the possible ETT-TTF molecule orientation has been drawn. a) View along the stacking axis *b* (dashed lines show S···S contacts shorter than 3.8 Å). b) View parallel to the long molecular axes of ETT-TTF molecules. c) Overlap mode of two consecutive ETT-TTF molecules within a stack. d) Overlap mode of two consecutive Au(mnt)$_2$ molecules within a stack.

generated from it by introducing one column of anions for every two columns of donors (see Figs. 4b,5b).

The IR and visible–near-infrared (vis-NIR) spectra of salt **4** are consistent with its mixed-valence character, showing the a_g vibrational modes of the donor and a broad "A band", characteristic of the mixed-valence states in low-dimensional conducting organic solids,[11] centered at 3680 cm^{-1}.

The electrical transport properties of salt **4** were studied by electrical conductivity and thermopower measurements performed on single crystals along their long axis, *b*. The electrical conductivity of (ETT-TTF)$_2$[Au(mnt)$_2$] (**4**) is thermally activated over the entire temperature range studied (150–300 K) with a room-temperature value of 3.6 S cm^{-1} and an almost-temperature-independent activation energy of 0.149 eV (Fig. 6). The electrical conductivity of this compound is reduced to about one half of that observed in the isostructural (DT-TTF)$_2$[Au(mnt)$_2$]. Furthermore, the ETT-TTF-based compound does not present any maximum in the apparent activation energy, in contrast to the DT-TTF-based compound, whose maximum at around 220 K was judged from diffuse X-ray scattering experiments to be attributed to a dimerization of the donor molecules along the chain axis, *b*.[4] Thermopower of the (ETT-TTF)$_2$[Au(mnt)$_2$] (**4**) in the temperature range 200–300 K decreases almost linearly upon cooling, as it does for the DT-TTF analogue, but with positive values reduced to almost one half (Fig. 7). This behavior is consistent with a hopping conduction mechanism between localized states with a finite density of states around the Fermi level, but without any transition resulting from dimerization, which is most likely prevented by disorder resulting from donor random orientation. The quality and size of crystals of salt **4** was not good enough to perform diffuse X-ray scattering experiments which could confirm this hypothesis.

The magnetic properties of salt (ETT-TTF)$_2$[Au(mnt)$_2$] (**4**) were studied by EPR and static magnetic-susceptibility measurements. The EPR spectrum of an oriented single crystal of **4** shows a single lorentzian resonance line with sinusoidal dependence on the angle of the applied magnetic field of both *g*-factor and peak-to-peak linewidth (ΔH_{pp}). The extreme values of both parameters are very similar to those found in (DT-TTF)$_2$[Au(mnt)$_2$] salt (Table 2),[4] in accordance with their isostructural characteristics. The slightly larger linewidth values found in (ETT-TTF)$_2$[Au(mnt)$_2$] are accounted for by the existence of more S···S contacts between radical cations (see structure description, above). The *g*-factor values agree with the orientation of (ETT-TTF)$^{+\bullet}$ molecules in the crystal, the minimum *g* value being observed when the external field (H_0) is applied perpendicular to the molecular plane. In this orientation, sulfur π-donor cation radicals have a very small spin–orbit contribution and the *g* factor coincides with that of the free electron (2.0023).[12] On the other hand, the maximum *g* value is found when H_0 is parallel to the *a**-crystallographic axis,

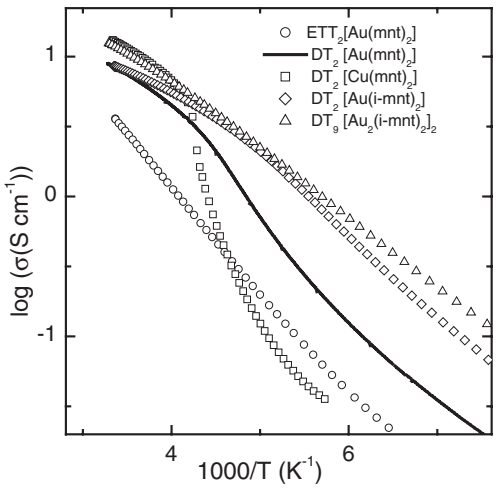

Figure 6. Plot of the logarithm of the electrical conductivity, log σ, as a function of the inverse of the temperature *T*, along the long axis of different single crystals: (ETT-TTF)$_2$[Au(mnt)$_2$] (**4**) (circles), (DT-TTF)$_2$[Au(mnt)$_2$] (line) [4a,b], (DT-TTF)$_2$[Cu(mnt)$_2$] (**8**) (squares), (DT-TTF)$_2$[Au(i-mnt)$_2$] (**5**) (diamonds), and (DT-TTF)$_9$[Au$_2$(i-mnt)$_2$]$_2$ (**6**) (triangles).

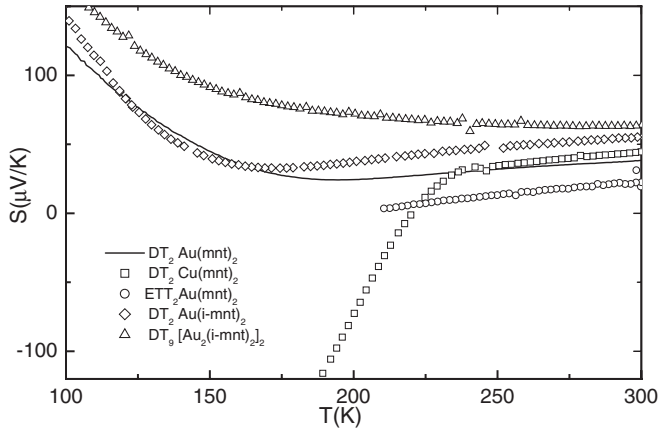

Figure 7. Absolute thermoelectric power (*S*), as a function of the temperature (*T*), measured along the long axis of different single crystals: (ETT-TTF)$_2$[Au(mnt)$_2$] (**4**) (circles), (DT-TTF)$_2$[Au(mnt)$_2$] (line) [4a,b], (DT-TTF)$_2$[Cu(mnt)$_2$] (**8**) (squares), (DT-TTF)$_2$[Au(i-mnt)$_2$] (**5**) (diamonds), and (DT-TTF)$_9$[Au$_2$(i-mnt)$_2$]$_2$ (**6**) (triangles).

which corresponds approximately to the longest axis of the molecule. The average *g*-factor value (2.0064) agrees with that found for the free radical cation (ETT-TTF)$^{+\bullet}$ in isotropic solution ($g_{iso} = 2.0069$), indicating that the signal is only due to the donor component of the salt, in accordance with the diamagnetic character of the counter-ion.

The static paramagnetic susceptibility (χ_p) of salt **4** was measured by the Faraday method after correction for the diamagnetic contribution, estimated to be 4.6×10^{-4} emu mol^{-1} (from tabulated Pascal constants), in the 4–300 K temperature range (see Fig. S2 in the Supporting Information). The large susceptibility value at room temperature (2×10^{-3} emu mol^{-1}), that gave an effective magnetic moment corresponding to one spin per formula unit, is consistent with the localization of electrons already at room temperature. This behavior is due to the strongly localized electrons in the ETT-TTF chains, in agreement with transport properties.

The magnetic susceptibility is dominated at low temperatures by a large Curie tail corresponding to 10 % $S = 1/2$ spins. Even considering this Curie tail, the temperature dependence of the susceptibility does not follow the expected spin-ladder behavior with a gap in the low temperature region. In contrast, the susceptibility is more consistent with the presence of antiferromagnetic interactions in various directions, which can be mediated by the diamagnetic anions. The absence of a spin-ladder magnetic behavior should be attributed to the disorder existent in the crystal structure of (ETT-TTF)$_2$[Au(mnt)$_2$] (**4**), that prevents the long-range dimer formation necessary to have uniformly localized spin-carrier units interacting in a ladder mode. This explanation is in agreement with the existence of a large Curie tail arising from defects in the crystals (10 % of $S = 1/2$ impurities).

It should be mentioned that among the different tetrathiafulvalene derivatives that we have been studying in recent years, ETT-TTF (**3**) is, so far, the only one that, when combined with the Au(mnt)$_2$ anion, presents a crystal structure similar to that of the (DT-TTF)$_2$[Au(mnt)$_2$] with a ladder arrangement of the donors. This donor when combined with Pt(mnt)$_2$ gives a Pt(III) salt with a distinct structure, and with Ni(mnt)$_2$, even a salt with a different stoichiometry (ETT-TTF)[Ni(mnt)$_2$].[13] All other donors, namely BET-TTF,[14,15] TTDM-TTF ((thiophene)(thiodimethylene)-tetrathiafulvalene),[16] BMDT-TTF (bis(methylenedithio)tetrathiafulvalene),[17] or EDT-TTF (ethylenedithiotetrathiafulvalene),[17] when combined with M(mnt)$_2$ complexes, give salts with completely different structures, and sometimes even with different stoichiometries.

2.2. Second Approach: Combination of the Same Donor, DT-TTF, with Another M-Dithiolene Ligand Complex

Since the disorder in the ETT-TTF donor causes the absence of long-range dimerization and consequently, prevents regular spin-ladder magnetic interactions, we decided to use the second approach to obtain new similar spin ladders: i.e., to combine the same DT-TTF donor and different counter-ions similar to Au(mnt)$_2$. At this point it should be mentioned that the previous combination of the DT-TTF organic donor with different gold dichalcogenide complexes gives salts with distinct crystal structures or even different stoichiometries, such as with pyrazine-2,3-dichalcogenate (DT-TTF)$_4$[Au(L)$_2$]$_3$ (L = pds, pdt)[18] or *N*-cyanodithiocarbamate (DT-TTF)[Au(cdc)$_2$].[19] Therefore, following this strategy, we decided to focus on complexes closer to Au(mnt)$_2$ and selected first the gold(III) complex of the iso-maleonitriledithiolate (1,1-dithio-2,2-dicyanoethylene), Au(i-mnt)$_2$,[20] since it has very similar shape and size to the previously used complex, Au(mnt)$_2$, as well as the same components for the supramolecular interactions in the crystal, that is, S atoms and C≡N groups. In addition, it has also a great tendency to form stacks and it has already been used to obtain metallic molecular compounds by combination with another aromatic donor, perylene.[21]

By electrocrystallization from solutions of the DT-TTF donor and the tetrabutylammonium salt of the monoanionic

Table 2. EPR parameters of different salts.

Compound	(DT-TTF)$_2$[Au(mnt)$_2$] [4a,b]	(ETT-TF)$_2$[Au(mnt)$_2$] (**4**)	(DT-TTF)$_2$[Au(i-mnt)$_2$] (**5**)	(DT-TTF)$_9$[Au$_2$(i-mnt)$_2$]$_2$ (**6**)	(DT-TTF)$_2$[Cu(mnt)$_2$] (**8**)	(DT-TTF)[Cu(mnt)$_2$] (**9**)
g_{max} (ΔH_{pp}, Gauss)	2.0131(43)	2.0161 (44)	2.0110 (40)	2.0083 (15)	2.0121 (42)	2.0145 (2.5)
g_{med} (ΔH_{pp}, Gauss)	2.0052 (26)	2.0051 (31)	2.0050 (33)	2.0040 (10)	2.0050 (25)	2.0050 (3.4)
g_{min} (ΔH_{pp}, Gauss)	2.0021 (25)	2.0024 (27)	2.0020 (26)	–	2.0021 (24)	2.0011 (1.8)

ADVANCED FUNCTIONAL MATERIALS

$[Au(i\text{-}mnt)_2]^-$ complex, different compounds were obtained and in most cases two or more crystalline phases grew in the same experiment.

When dichloromethane was used as the solvent for the electrocrystallization, crystals of $(DT\text{-}TTF)_2[Au(i\text{-}mnt)_2]$ (**5**) were obtained as dark black–green plates that grew on the platinum electrode in the form of date-palm leaves. Nevertheless, in only a few experiments was salt **5** obtained as the unique or principal component. For all solvents used (CH_3CN, CH_2Cl_2, C_6H_5Cl, tetrahydrofuran (THF), $CHCl_3$, trichloroethane, tetrachloroethane, CH_2Cl_2/EtOH, $CH_2Cl_2/CHCl_3$, and CH_2Cl_2/CCl_4), small black needles corresponding to a salt with formula $(DT\text{-}TTF)_9[Au_2\text{-}(i\text{-}mnt)_2]_2$ (salt **6**), as ascertained by elemental analysis, were formed either as a majority compound (for CH_3CN, THF, C_6H_5Cl) or as contaminant of other phases. Thus, salt **5** is usually obtained as a mixture with salt **6**, despite many different experiments changing the temperature, current intensity, donor/electrolyte proportion, humidity, etc, were performed.

Furthermore, when using CH_3CN as the solvent, and only in some experiments, jet-black squared-shaped single crystals of another compound, $(DT\text{-}TTF)_2[Au_2(i\text{-}mnt)_2]$ (salt **7**), grew on the anode together with small needles of salt **6**.

Unfortunately, none of the small black needles of the most abundant phase of $(DT\text{-}TTF)_9[Au_2(i\text{-}mnt)_2]_2$ (salt **6**) were found to be good enough to solve the crystal structure. The physical properties of this compound are currently under study, as well as structural X-ray diffraction (XRD) studies in powder to corroborate the stoichiometry tentatively assigned using the elemental analysis and energy-dispersive X-ray (EDX) data.

In contrast, salt **7** was characterized using single-crystal X-ray crystallography (Table 1). The crystal structure shows that the anion included in the compound is not the initial one as in salt **5**, but the binuclear gold(I) complex of the isomaleonitriledithiolate ligand, $[Au_2(i\text{-}mnt)_2]^{2-}$, as also found in salt **6** by elemental and EDX analysis. This modification in the anion had been already found in the electrocrystallization from the BEDT-TTF (bis(ethylenedithio)tetrathiafulvalene) donor with the same $(n\text{-}Bu_4N)[Au(i\text{-}mnt)_2]$ salt, which yields crystals of the $(BEDT\text{-}TTF)_2[Au_2(i\text{-}mnt)_2]$ compound on the platinum electrode,[22] and it is generated by electrocrystallization and other redox processes.[23] The new complex anion contains two gold atoms homo-bridged by the dithiolate ligand in which the two gold atoms are at a separation of 2.779(2) Å, well within the range of the aurophilic bonding.[24] Compound **7** crystallizes in the tetragonal chiral space group $P4_32_12$. An Oak Ridge Thermal Ellipsoid Plot Program (ORTEP) drawing of the asymmetric unit is shown in Figure S3 (Supporting Information).

The DT-TTF molecules are almost planar (Fig. 8), whereas the gold complex has a torsion angle with respect the Au–Au bond of –11.1° (Fig. 8 and Fig. S3 in the Supporting Information). The chirality of the structure comes from this torsion since only one of the two possible torsion senses is present in the crystal structure. It is worth noting that the torsion found in the $[Au_2(i\text{-}mnt)_2]^{2-}$ dianion, that finally yields to the chiral structure, is reported here for the first time.[22,23] The crystal

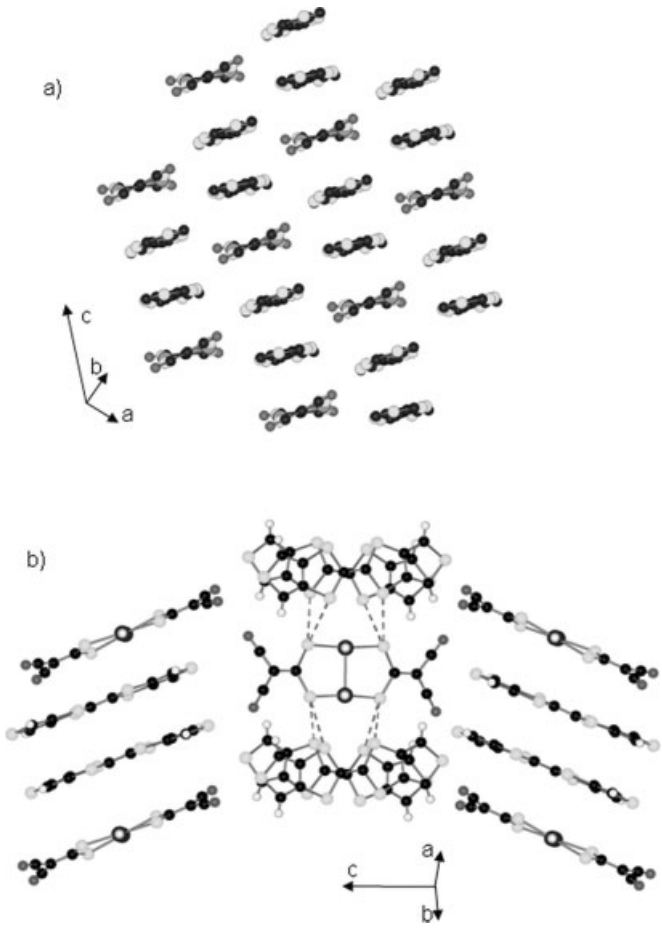

Figure 8. Crystal structure of $(DT\text{-}TTF)_2[Au_2(i\text{-}mnt)_2]$ (**7**). a) View of one sheet of dimers and anions. b) View of the alternation of sheets along the *c*-axis (dashed lines show S···S contacts shorter than 3.52 Å).

packing shows that each divalent anion is associated with four DT-TTF radical cations that in turn are associated, forming dimers with very short intradimer S···S contacts of 3.372 and 3.536 Å. These dimers are also chiral since they form an angle of 16.7° between their central C=C bonds, and their chirality is promoted by the strong S···S interactions with the anion, the sulphur atoms being at distances of 3.333, 3.521, 3.402, and 3.490 Å, all much shorter than the sum of the van der Waals radii (3.6 Å) (Fig. 8).

Stacks of two dimerized DT-TTF molecules and one anion are observed along $a+b$, forming alternated chains of one dimer and one anion (Fig. 8a), and generating, in that way, a sheet almost perpendicular to the next one along the *c*-axis (Fig. 8b).

In accordance with the completely ionic character of the donors in salt **7**, the vis-NIR spectrum shows only the characteristic B band centered at 850 nm. On the other hand, the strong dimerization of the DT-TTF cation radicals leads to an almost diamagnetic behavior for **7**. The $(DT\text{-}TTF)_2[Au_2(i\text{-}mnt)_2]$ salt displays a very weak EPR signal that is attributed to some defects in the crystals, in accordance with the existence of strong antiferromagnetic interactions in the dimers.

The introduction of chirality in TTF-based materials has been a matter of important attention in the past decade, and relevant results have been achieved in the search for multifunctional chiral and conducting materials. The structure of **7** may open new approaches in this direction if we can take advantage of the torsion of the $[Au_2(i\text{-}mnt)_2]^{2-}$ dianion, in order to spread the chirality to an organic TTF-based conducting network.[25]

We will concentrate now on salt **5**, which has the desired formula for achieving a spin-ladder magnetic behavior. The crystal structure of (DT-TTF)$_2$[Au(i-mnt)$_2$] (**5**) was determined by single-crystal XRD. For the solved structure, the collection data and crystal parameters of **5** are given in Table 1. The asymmetric unit of compound **5** is depicted in Figure S4 (Supporting Information).

Salt **5** crystallizes in the monoclinic space group $P2_1/n$, being isostructural with the (DT-TTF)$_2$[Au(mnt)$_2$][4a,b] and (ET-TTF)$_2$[Au(mnt)$_2$] (**4**) salts (Table 1), with virtually undistinguishable molecular packing structure (see Figs. 2b,5a,b and Fig. S5 in the Supporting Information). A comparison of the molecular interplanar distances, angles, and short contacts with the other isostructural ladder compounds is shown in Table S1 (Supporting Information).

Electrical conductivity measurements on a single crystal of salt **5** along the chain-axis-*b* (Fig. 6) show an activated behavior comparable to that of the Au(mnt)$_2$ salt with a slightly larger room-temperature value of 15 S cm^{-1}, and an apparent activation energy also with a broad maximum ~200 K, suggesting an equal onset of localization at this temperature. Thermopower measurements of **5** also reveal a behavior equally comparable to the Au(mnt)$_2$ analogue salt (Fig. 7).

Both the structural characteristics and the electronic-transport properties suggest magnetic properties with spin-ladder behavior, comparable to that of (DT-TTF)$_2$[Au(mnt)$_2$]. If the electrons become localized in dimers of DT-TTF molecules formed along the stacks, these $(DT\text{-}TTF)_2^{+\bullet}$ dimers will constitute the spin-carrying units in a spin ladder.

Magnetic properties of salt **5** were studied only using EPR spectroscopy, since it was not possible to obtain a quantity of pure sample large enough to perform static magnetic-susceptibility measurements. As explained before, more than one salt is obtained in each electrocrystallization experiment and, therefore, the single crystals of the ladder-like phase of (DT-TTF)$_2$[Au(i-mnt)$_2$] (salt **5**) had to be carefully selected individually in order to perform the EPR measurements. Under these circumstances, EPR spectroscopy was very useful to distinguish between different phases since their EPR parameters, especially the peak-to-peak linewidth (ΔH_{pp}), are quite different ($g = 2.0083$, $\Delta H_{pp} \sim 25$G for compound **7**; see Table 2 for EPR data of **5** and **6**), as expected for dissimilar supramolecular organization of the donor molecules in the crystal.

The EPR characteristics of salt **5** are very similar to those of the isostructural (DT-TTF)$_2$[Au(mnt)$_2$][4a,b] and (ETT-TTF)$_2$-[Au(mnt)$_2$] (**4**) salts (Table 2). The thermal variation of the *g* factor, peak-to-peak linewidth (ΔH_{pp}), and signal intensity (*I*), observed when an external field is applied perpendicular to the needle axis of several selected crystals of **5**, were studied. Both the *g* factor and ΔH_{pp} did not exhibit appreciable changes upon cooling, but the signal intensity, which is proportional to the paramagnetic susceptibility, exhibited a variation comparable to that previously observed in (DT-TTF)$_2$[Au(mnt)$_2$] (Fig. 9). This spin susceptibility exhibits a maximum around 75 K with an activated behavior below this temperature, which is characteristic of a system with localized spins interacting antiferromagnetically and displaying a gap in the spin excitations, as in a spin ladder. Below 10 K an increase of intensity due to a small Curie tail is observed.

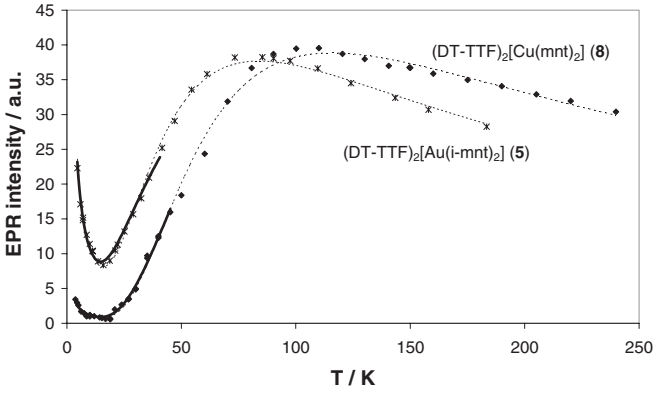

Figure 9. EPR spin susceptibility of (DT-TTF)$_2$[Au(i-mnt)$_2$] (**5**, stars) and (DT-TTF)$_2$[Cu(mnt)$_2$] (**8**, diamonds) as a function of temperature. The solid line is a fit with Equation 1 using the Troyer χ_{ladder} Equation 2, and the dotted line is a fit using the Barnes and Riera χ_{ladder} Equation 3 (see text), in both compounds **5** and **8**.

Accordingly, it is possible to fit the susceptibility data to Equation 1,

$$\chi = f\chi_{ladder} + (1-f)\chi_{Curie} \quad (1)$$

in which further to a Curie component, χ_{Curie}, which takes into account both the magnetic defects in the crystals and the finite sizes of the ladders, there is a major contribution χ_{ladder}, due to the spin ladders. This last contribution at low temperatures, where there is an exponential decay of susceptibility upon cooling (from 4 to 40 K in this case), is expected to be well approximated by the Troyer expression (Eq. 2) for a two-legged spin-ladder system,[26]

$$\chi_{ladder} = \alpha T^{-1/2}\exp(-\Delta/kT) \quad (2)$$

where α is a constant corresponding to the dispersion of the excitation energy and Δ is the finite energy gap in the spin–excitation spectrum.

Alternatively, in a more extended temperature range, χ_{ladder} is a function of the exchange interactions along the legs ($J_{\|}$) and the rungs ($J_{\perp}$) of the ladder, that can be approximated by Equation 3, given by Barnes and Riera,[2b]

$$\chi_{ladder}(T) = \frac{c_1}{T}\left[1 + \left(\frac{T}{c_2}\right)^{c_3}(e^{c_4/T} - 1)\right]^{-1}\left[1 + \left(\frac{c_5}{T}\right)^{c_6}\right]^{-1} \quad (3)$$

where $c_1 = g^2\mu_B{}^2/4k_B$ and c_2, c_3, c_4, c_5 and c_6, depend on $J_{\perp}$ and $J_{\|}$.

ADVANCED FUNCTIONAL MATERIALS

As shown in Figure 9, both equations can fit our data accurately. With Equation 2 (dotted line) the best fit was obtained with $f = 0.971$ and $\Delta/k_B = 71$ K ($r^2 = 0.972$). With Equation 3 the best fit in the temperature range 4–185 K corresponds to $J_{\|}/k_B = 86$ K, $J_{\perp}/k_B = 142$ K with the same f ($r^2 = 0.986$).

Thus, the temperature dependence of the magnetic susceptibility clearly shows that the (DT-TTF)$_2$[Au(i-mnt)$_2$] salt is a purely organic molecular system with a two-legged-spin-ladder magnetic configuration.

Remarkable in this two-legged spin ladder is the fact that the $J_{\perp}/J_{\|}$ ratio is 1.65, which is close to that of an ideal spin ladder.[27] The spin gap has also been calculated from the resulting values of $J_{\|}$ and $J_{\perp}$ with the theoretical Equation 4,[26]

$$\Delta = J_{\perp} - J_{\|} + J_{\|}^2/2J_{\perp} \quad (4)$$

giving $\Delta/k = 82$ K, a value that is of the same order of magnitude of that found with Equation 2.

These results characterize (DT-TTF)$_2$[Au(i-mnt)$_2$] as the second example of a spin ladder, with the [(DT-TTF)$_2^{+\bullet}$] as spin-carrying unit and with very similar exchange parameters and spin-gap value to the previously known example, the (DT-TTF)$_2$[Au(mnt)$_2$] compound (see Table 3).[4a]

The last change we have introduced following the second strategy, i.e., modification on the anion, has been even smaller since we have only replaced the Au metal (M) in the M(mnt)$_2$ complex by Cu, in order to preserve the diamagnetic character of the anion. The Cu(mnt)$_2^-$ anion has been already combined with the perylene donor to give a molecular metal[28] belonging to a family with a structure[29] quite similar to the (DT-TTF)$_2$-M(mnt)$_2$ compounds with M = Au, Ni, or Pt. However, due to the instability of the Cu mono-anionic complex in solution, the electrocrystallization essays were conducted using larger currents and during shorter periods of time than before, since, typically, 5–8 days easily leaded to decomposition of the anion.

By electrocrystallization from solutions of DT-TTF and the tetrabutylammonium salt of the copper(III) complex of maleonitriledithiolate, (n-Bu$_4$N)[Cu(mnt)$_2$], two compounds were obtained as dark needle-shaped crystals. One, with a metallic-like sheen is the (DT-TTF)$_2$[Cu(mnt)$_2$] (**8**) salt, and the other, less shiny, is a 1:1 salt, (DT-TTF)[Cu(mnt)$_2$] (**9**), that is favored under larger current densities. Nevertheless, we have not been able to accumulate large amounts of completely pure samples of neither of these salts.

The crystal structure of (DT-TTF)[Cu(mnt)$_2$] (**9**) is monoclinic, space group $P2_1/c$ and it consists in regular stacks of donors and acceptors parallel to the a-axis, which alternate in the b,c-plane (Fig. 10). A detailed structural description of the asymmetric unit can be found in Figures S7,S8 in the Supporting Information.

The bond lengths of the Cu complex are identical to those previously found in this monoanionic complex, either in ammonium salts as (n-Bu$_4$N)[Cu(mnt)$_2$],[30] or in charge-transfer salts with organic donors,[28b] and also in **8** (see below). The bond lengths of the donor are close to those expected for cationic DT-TTF, with a central C=C bond length of 1.393(14) Å, longer than that found in (DT-TTF)$^{1/2+}$ (1.370(7) Å) and also than that in the neutral donor (1.348 Å). The EPR parameters are in accordance with the low-dimensional electronic character of this salt, since a narrow line ($\Delta H_{pp} \sim 2$G) is observed, with g values typical of the DT-TTF cation, as expected for a Cu(III) diamagnetic salt.

The EPR signal is very weak, denoting a strong antiferromagnetic interaction of the DT-TTF radical cations. The intensity variation in the temperature range 4–300 K of several crystals of salt **9** shows a very smooth decrease of the paramagnetic signal from room temperature to ~50 K, where the signal becomes dominated by a Curie tail (Fig. S9 in the Supporting Information).

On the other hand, the crystal structure of (DT-TTF)$_2$-[Cu(mnt)$_2$] (**8**) shows that it is isostructural with the analogues (DT-TTF)$_2$[M(mnt)$_2$] (M = Au, Ni, and Pt) previously reported,[4a,31] as well as with salts **4** and **5** here described (Table 1 and Figs. 2b,5a,b), with virtually undistinguishable molecular packing structure (see Figs. S10,S11 in the Supporting Information). The main differences are the slightly smaller lattice parameters of the Cu salt as a consequence of the smaller metal atom. The molecular interplanar distances are also smaller than in the Au analogue (Table S1 in the Supporting Information).

Electrical conductivity and thermopower measurements on single crystals of (DT-TTF)$_2$[Cu(mnt)$_2$] (**8**) reveal a semiconducting behavior comparable to the Au analogue with a slightly larger electrical conductivity at room temperature, $\sigma_{RT} \sim 12$ S cm^{-1}, and comparable thermopower $S_{RT} = 45$ μV K^{-1} (Figs. 6,7, respectively). However, upon cooling there is a sharp second-order phase transition at 235 K, seen both on electrical resistivity (as a sharp maximum on the apparent activation energy) and in thermopower.[32] This transition was not present in

Table 3. Magnetic fitting parameters.

	(DT-TTF)$_2$[Au(mnt)$_2$] [4a,b]	(DT-TTF)$_2$[Au(i-mnt)$_2$] (**5**) EPR data	(DT-TTF)$_2$[Cu(mnt)$_2$] (**8**) EPR data
Δ/k_B (Eq. 2 ($T < 50$ K))	78	71	123
f (Eq. 2)	0.98	0.971	0.980
R^2 (Eq. 2)	0.997	0.972	0.992
$J_{//}/k_B$ (Eq. 3)	82	86	121
$J_{\perp}/k_B$ (Eq. 3)	142	142	218
Δ/k_B (Eq. 4)	83	82	130.6
f (Eq. 3)	0.98	0.971	0.980
R^2 (Eq. 3)	0.999	0.986	0.998

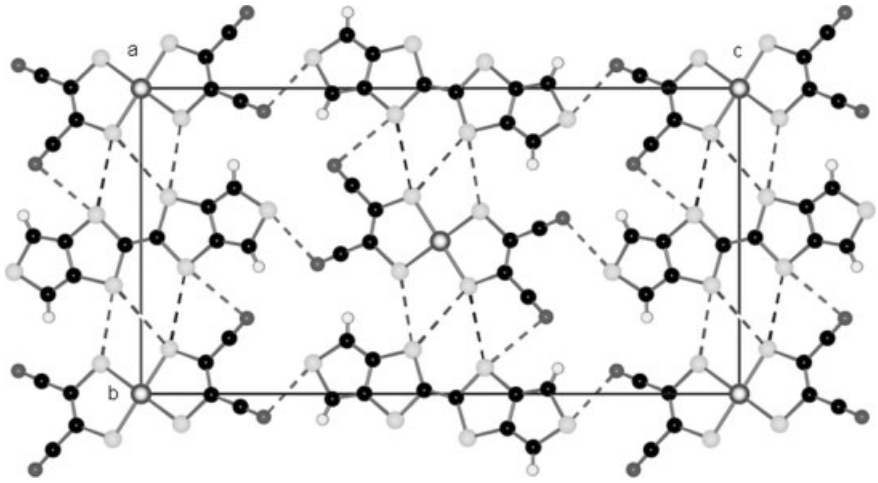

Figure 10. View of the crystal structure of (DT-TTF)[Cu(mnt)$_2$] (**9**) along *a*.

the Au analogue where only a broad localization was detected around 220 K.[4a,b]

The nature of this transition was investigated by diffuse X-ray measurements using the so-called fixed film-fixed crystal method and monochromatized Cu $K\alpha$ (λ = 1.542 Å) radiation as in previous studies on (DT-TTF)$_2$-M(mnt)$_2$ compounds,[31] which were performed at temperatures just below (200/220 K) and above (260 K) the transition (T_c = 235 K). The X-ray pattern at 260 K showed long diffuse segments located half way between b^* stratus. These results clearly correspond to pseudo-1D structural fluctuations correlated in the ladder direction (the *b*-axis) and decoupled between ladders. Below T_c, the diffuse segments condense into satellite reflections at the reduced wave vector q = (0, 1/2, ?) (Fig. S12 in the Supporting Information). This indicates a duplication of the unit cell along the stack direction.

These X-ray scattering results are similar to those obtained for the Au analogue.[4a,b] However, in the Au compound no long range order was observed, which could be attributed to the intrinsic low quality of the Au crystals. In both systems, a priori being quarter filled, the electronic and structural instability could be related to a $4k_F$ charge density wave (CDW) instability leading to the localization of the electrons and favoring the spin-ladder magnetic behavior at low temperature. The unexpected semiconducting behavior observed above T_c could be related to the formation of a pseudo-gap associated with the extended pseudo-1D structural fluctuations. Both the structural characteristics and the localization of electrons favors the spin-ladder behavior at low temperatures, similarly to those of (DT-TTF)$_2$[Au(mnt)$_2$] and (DT-TTF)$_2$[Au(i-mnt)$_2$] (**5**), if the electrons are localized in dimers of DT-TTF donors formed along the stacks. These dimers [(DT-TTF)$_2^{\bullet+}$] will constitute the spin-carrying units of the spin ladder.

Magnetic properties of salt **8** were properly studied by EPR spectroscopy and static magnetic susceptibility measurements. Similarly to salt **5**, good results were obtained only by EPR due to the impossibility of accumulating a large enough quantity of pure material free of the 1:1 salt (DT-TTF)[Cu(mnt)$_2$] (**9**) to perform static magnetic measurements. EPR characteristics of salt **8** are very similar to those of the isostructural (DT-TTF)$_2$[Au(mnt)$_2$], and salts **4** and **5** (Table 2), the minimum *g* value of the single resonance line being observed when the external field (H_0) is applied along the perpendicular axis of the DT-TTF molecular plane, and the maximum when the field is applied along the crystallographic a^*-axis. In Figure 9, the thermal variation of the signal intensity (*I*) observed when the external field is applied perpendicular to the needle axis of several selected crystals of **8** is displayed. It exhibits a maximum around 85 K with an activated behavior below this temperature, which is very similar to that of (DT-TTF)$_2$-[Au(mnt)$_2$] and (DT-TTF)$_2$[Au(i-mnt)$_2$] (**5**) salts, with a smaller, almost negligible, Curie tail. This EPR susceptibility data could be well fitted by Equations 2 and 3 in a similar way as done previously for the salt **5**, with the parameters listed in Table 3. The fitting is of comparable quality, but the parameters obtained, f = 0.980 and Δ/k = 123 K (r^2 = 0.992, T_{Range} = 4–45 K) for Equation 2, and $J_\parallel/k_B$ = 121 K, $J_\perp/k_B$ = 218 K with the same f (r^2 = 0.998, T_{Range} = 4–240 K) for Equation 3, are, in general, slightly larger, as expected from the smaller intermolecular distances which predict larger magnetic interactions.

The spin gap has also been calculated from the resulting values of $J_\parallel$ and $J_\perp$ with the theoretical Equation 4, giving Δ/k = 130.6 K, which is in agreement with the previous value calculated from the Troyer expression (Eq. 2). A remarkable aspect of this two-legged spin ladder, the third one of the family, is the fact that the $J_\perp/J_\parallel$ ratio is 1.75, similar to the case of **5**, which is also close to that of an ideal spin ladder.

3. Conclusions

A systematic effort to obtain organic spin ladders of the same family, closely related by small molecular and structural changes, was successfully undertaken for the first time. Using (DT-TTF)$_2$[Au(mnt)$_2$] as the prototype reference spin-ladder system, we found that, through only minor modifications in the DT-TTF donor or in the Au(mnt)$_2^-$ anionic complex, it is possible to preserve the ladder structure and afford compounds isostructural to (DT-TTF)$_2$[Au(mnt)$_2$].

In spite of being isostructural, the small disorder in the donor ladder structure of (ETT-TTF)$_2$[Au(mnt)$_2$] (**4**), formed with the DT-TTF-related donor ETT-TTF, was found to be enough to prevent the formation of the dimeric spin-carrying units and thus avoiding the magnetic spin-ladder behavior. Other variations in the donor led to quite different structures.[15,16]

On the contrary, two new spin-ladder compounds, (DT-TTF)$_2$-[Au(i-mnt)$_2$] (**5**) and (DT-TTF)$_2$[Cu(mnt)$_2$] (**8**), were obtained by introducing small changes in the anionic complex; even

ADVANCED FUNCTIONAL MATERIALS

though the typical ladder structure was found to be rare, being just one of the various possible structures when combining DT-TTF with bisdithiolate metal complexes. The ladder-like compound **5** resulted from the change of the mnt ligand of the complex for its isomeric ligand i-mnt, both bearing the same S and CN interacting groups with very similar size and shape structure, and, therefore, very similar $J_{\parallel}$ and $J_{\perp}$ values were obtained. The variation in compound **8** is only with regard to the metal, now the copper replacing the gold atom. The smaller size of copper compared to gold allows for a closer packing of the donors with enhanced magnetic interactions, an effect that is reflected in the higher values of $J_{\parallel}$ and $J_{\perp}$. Noteworthy, both new spin ladders **5** and **8** reported in this paper present a $J_{\perp}/J_{\parallel}$ ratio of 1.65 and 1.75, that are very close to that of the ideal spin-ladder systems ($J_{\perp}/J_{\parallel} \sim 1$).

The very minor chemical variations that are allowed for keeping the spin-ladder magnetic properties reveal the enormous difficulty in synthesizing such compounds and thus, the high relevance of describing the family of spin-ladder compounds reported.

4. Experimental

The synthesis of 5,6-dihydrothieno[2,3-*d*]-1,3-dithiol-2-one [8] and thieno[3,4-*d*]-1,3-dithiol-2-thione [6] was performed as previously described. The (n-Bu_4N)[$M(mnt)_2$] (M = Au, Cu) and (n-Bu_4N)[$Au(i\text{-}mnt)_2$] salts were also prepared and purified by recrystallization as previously described [20,33,34].

FT-IR spectra were recorded on a Nicolet 710 spectrophotometer on KBr disks. ^{1}H NMR and ^{13}C NMR spectra were measured in a Bruker Aspect 3000 at 300 MHz for ^{1}H and 75.5 MHz for ^{13}C with tetramethylsilane (TMS) as internal reference. UV-vis-NIR absorption spectra were obtained on a Varian Cary 5 spectrophotometer. Melting points were determined on a Perkin–Elmer DSC 7.

X-ray data for single crystals of ETT-TTF (**3**), $(ETT\text{-}TTF)_2[Au(mnt)_2]$ (**4**), and (DT-TTF)[$Cu(mnt)_2$] (**9**) were collected on an Enraf Nonius CAD4 diffractometer with monochromatic Mo $K\alpha$ radiation ($\lambda = 0.71073$ Å). X-ray data for single-crystal $(DT\text{-}TTF)_2[Cu(mnt)_2]$ (**8**) were collected on a TURBO CAD4-Enraf Nonius diffractometer with monochromatic Cu $K\alpha$ radiation ($\lambda = 1.5415$ Å). The cell parameters were determined from a least-squares refinement of twenty-five reflections randomly searched. Data were collected by using a ω-2θ scan method. The MolEN [35] package was used for applying Lorentz-polarization and Ψ-scan empirical absorption corrections. The structures were solved by direct methods using SHELXS97 [36] or SIR97 [37] programs and refined by a full-matrix least-squares method using SHELXL97 program [38]. Least-squares calculation minimized $\Sigma w(\Delta F)^2$, being $w = [\sigma^2(F_0^2) + (a \cdot P)^2 + b \cdot P]^{-1}$, $P = (F_0^2 + 2F_c^2)/3$. Non-H atoms were anisotropically refined and H-atoms were positioned in calculated positions and refined with a global isotropic temperature factor.

X-ray data for single crystals of $(DT\text{-}TTF)_2[Au(i\text{-}mnt)_2]$ (**5**) and $(DT\text{-}TTF)_2[Au_2(i\text{-}mnt)_2]$ (**7**) were collected on a Nonius Kappa charge-coupled device (CCD) diffractometer with monochromatic Mo $K\alpha$ ($\lambda = 0.71073$ Å) radiation. Data were collected via ϕ and ω multiscans and reduced with the program DENZO-SMN without absorption correction. Measured reflections were corrected with the program SCALEPACK. The structure was refined by a full-matrix least-squares method using SHELXL-93. Least-squares calculation minimized $\Sigma w(\Delta F)^2$, being $w = [\sigma^2(F_0^2) + (a \cdot P)^2 + b \cdot P]^{-1}$, $P = (F_0^2 + 2F_c^2)/3$. Crystal parameters, data-collection details, and results of the refinements are summarized in Table 1.

Crystallographic data (excluding structure factors) for the structures of compounds **3**, **4**, **5**, **7**, **8**, and **9** reported in this paper have been deposited with the Cambridge Crystallographic Data Centre as supplementary publication no. CCDC 249497–249502, respectively. Copies of the data can be obtained free of charge via www.ccdc.cam.ac.uk/conts/retrieving.html or on application to The Director, CCDC, 12 Union Road, Cambridge CB2 1EZ, UK; fax: (+44) 1223 336 033; e-mail: deposit@ccdc.cam.ac.uk.

Electrical conductivity and thermoelectric power measurements were performed in the range 175–320 K in the same sample in order to avoid possible confusion between different phases. In a first step thermopower was measured using a slow AC ($\sim 10^{-2}$ Hz) technique by attaching to the extremities along the larger dimension of the crystals with platinum paint (Demetron 308A), two $\phi = 25$ μm 99.99 % pure-Au wires (Goodfellow Metals) anchored to two quartz thermal reservoirs, in a previously described apparatus [39], controlled by a computer [40]. The oscillating thermal gradient was kept below 1 K, and it was measured with a differential Au–0.05 at.-% Fe versus chromel thermocouple. The sample temperature was measured by a previously calibrated thermocouple of the same type. Both the differential thermocouple and the sample voltage were measured with Keithley 181 nanovoltmeters. The absolute thermopower of the sample was obtained after correction for the absolute thermopower of the Au leads, using the data of Huebner [41]. In a second step, electrical resistivity measurements were performed in the same sample using a four-probe technique. Without removing the crystal from the sample holder, two extra Au wires were placed on the sample in order to achieve a four-in-line contact configuration. Prior to the measurements the sample was checked for un-nested to nested voltage ratio, as defined by Schafer et al. [42], that was below 5 %. Measurements were done imposing through the sample a current of 1 μA at low frequency (77 Hz) and measuring the voltage drop with a lock-in amplifier.

EPR Spectra in the range 4–300 K were obtained with an X-Band Bruker ESP 300E spectrometer equipped with a rectangular cavity operating in T102 mode, a Bruker variable-temperature unit and an Oxford EPR-900 cryostat, a field-frequency lock ER 033M system and a NMR Gaussmeter ER 035M. The modulation amplitude was kept well below the linewidth and the microwave power was well below saturation.

*Synthesis of ETT-TTF (**3**)*: A solution of 5,6-dihydrothieno[2,3-*d*]-1,3-dithiol-2-one (**1**) (0.180 g, 1.02 mmol) and thieno[3,4-*d*]-1,3-dithiol-2-thione (**2**) (0.380 g, 1.99 mmol) in freshly distilled trimethyl phosphite (9 mL) were heated to reflux in an argon atmosphere for 20 h. After cooling to room temperature, the formed precipitate was filtered off, washed with ether, and dried (under vacuum) to yield a orange microcrystalline solid (0.163 g) containing ETT-TTF, DT-TTF, and a small quantity of BET-TTF. The mixture was chromatographed on silica gel eluting with carbon disulfide to afford ETT-TTF (0.078 g, 24 %) as a yellow–orange powder: melting point (mp) 187.9 °C (dec.), onset at 186.6 °C; ^{1}H NMR (d_6-dimethylsulfoxide (DMSO)): δ 6.85 (s, 2H, C$\underline{H}$–S), 3.73 (t, 2H, $J = 8.4$ Hz, C$\underline{H}_2$–C), 2.83 (t, 2H, $J = 8.4$ Hz, CH$_2$–S$\underline{H}_2$); ^{13}C NMR: (d_6-DMSO) δ 135.9 (CH–$\underline{C}$–S), 125.6 (CH$_2$–CH$_2$–S–$\underline{C}$–S), 122.3 (CH$_2$–CH$_2$–$\underline{C}$–S), 112.1 (S–$\underline{C}$H–C), 38.4 (S–$\underline{C}$H$_2$–CH$_2$), 32.9 (CH$_2$–$\underline{C}$H$_2$–C); IR (KBr): 3906, 2968, 2932, 2910, 1423, 1319, 1296, 1153, 1018, 831, 763, 744, 700, and 495 cm^{-1}; UV-vis ($CHCl_3$) λ_{max} (log ε): 443 (2.55), 329 (4.17), 296 (4.14) nm; mass spectrometry (MS) *m/e* [%]: 318 (M^+, 100), 69 (C_3HS^+, 22); Anal. Calcd. for $C_{10}H_6S_6$: C, 37.71; H, 1.90; S, 60.39 %. Found: C, 37.75; H, 1.95; S, 60.21 %.

Crystals suitable for X-ray determination were obtained by a slow evaporation of a dichloromethane solution of ETT-TTF at room temperature.

*Synthesis of $(ETT\text{-}TTF)_2[Au(mnt)_2]$ (**4**)*: $(ETT\text{-}TTF)_2[Au(mnt)_2]$ crystals were obtained by electrocrystallization from dichloromethane solution of the ETT-TTF donor and the tetrabutylammonium salt of $[Au(mnt)_2]^-$ as electrolyte, in approximately stoichiometric amounts, with Pt electrodes and at a constant current of 0.2 μA. After one week, brown plate-shaped crystals were obtained.

*Synthesis of $(DT\text{-}TTF)_2[Au(i\text{-}mnt)_2]$ (**5**)*: crystals of salt **5** were obtained by electrocrystallization from dichloromethane 99.9 % high-performance liquid chromatography (HPLC)-grade purchased from Aldrich, of the DT-TTF donor and the tetrabutylammonium salt of $[Au(i\text{-}mnt)_2]^-$ as electrolyte. An electrolyte solution of 4.258 mg of (n-Bu_4-

N)[Au(i-mnt)$_2$] in 12.5 mL of CH_2Cl_2 was prepared. A solution prepared with 2.05 mg of DT-TTF and 0.868 mg of tetraiodoethylene (I_4C_2) dissolved in 6.5 mL of the electrolyte solution was placed in the anode compartment. The other 6 mL of electrolyte solution were immediately placed in the cathode compartment. The system was sealed under argon, and a constant current intensity of 1 μA was applied for five days. Black–dark-green palm-leaf-shaped crystals grown on the anode correspond to the spin-ladder compound (DT-TTF)$_2$[Au(i-mnt)$_2$]. The molar relation of the species was DT-TTF/Au(i-mnt)$_2$/I_4C_2 = 1.00:1.26:0.25 . It has to be noted that this synthesis is poorly reproducible, and mixture of **5** with other phases (compounds **6** and **7**) are usually found.

*Synthesis of (DT-TTF)$_9$[Au$_2$(i-mnt)$_2$]$_2$ (**6**)*: crystals of salt **6** were obtained as the most abundant crystal phase in most of the electrocrystallization experiments performed in order to obtain the spin ladder (DT-TTF)$_2$[Au(i-mnt)$_2$] (**5**), using a wide range of solvents and constant current intensities. Anal. Calcd. for $C_{106}H_{36}S_{62}N_8Au_4$: C, 30.33; H, 0.86; N, 2.67; S, 47.36 %. Found: C, 30.57; H, 0.99; N, 2.80; S, 47.21 %. EDX analysis indicated an S/Au atomic ratio of 13.4 ± 0.7 (theoretical S/Au = 15.5 for 9:2 stoichiometry).

*Synthesis of (DT-TTF)$_2$[Au$_2$(i-mnt)$_2$] (**7**)*: crystals of salt **7** were obtained by electrocrystallization from CH_3CN HPLC-grade purchased from SDS. An electrolyte solution of 3.10 mg of (*n*-Bu_4N)[Au(i-mnt)$_2$] in 12 mL of CH_3CN was prepared. A solution prepared with 3.54 mg of DT-TTF dissolved in 6 mL of the electrolyte solution was placed in the anode compartment. The other 6 mL of electrolyte solution were immediately placed in the cathode compartment. The system was sealed under argon, and a constant current intensity of 1 μA was applied for four days. Jet-black squared-shaped crystals grown on the anode correspond to the compound (DT-TTF)$_2$[Au$_2$(i-mnt)$_2$] (**7**). However, the most abundant phase of this experiment was characterized by EPR as compound **6**. The molar relation of the species was DT-TTF/Au(i-mnt)$_2$ = 1.88:1.00.

*Synthesis of (DT-TTF)$_2$[Cu(mnt)$_2$] (**8**)*: crystals of salt **8** were obtained by electrocrystallization, at room temperature, from dichloromethane solutions (Lab-Scan p.a.), of the DT-TTF donor and the tetrabutylammonium salt of [Cu(mnt)$_2$]$^-$ as electrolyte, which was prepared and purified as described before [33,34]. A solution of 9.0 mg of DT-TTF in 7.5 mL of CH_2Cl_2 was placed in the anode compartment. Immediately after an electrolyte solution of 8.3 mg of (*n*-Bu_4N)[Cu(mnt)$_2$] in 7.5 mL of CH_2Cl_2 previously prepared was placed in the cathode compartment. The system was sealed under argon, and a constant current intensity of 7 μA was applied for 36 h. Black needle-shaped crystals, with metallic sheen, were grown on the anode which corresponds to (DT-TTF)$_2$[Cu(mnt)$_2$]. A variable amount of (DT-TTF)[Cu(mnt)$_2$] (**9**), also black but without the metallic shine, is found mixed with these crystals.

*Synthesis of (DT-TTF) [Cu(mnt)$_2$] (**9**)*: A preparation of **9** was obtained by electrocrystallization under conditions similar to those described above for **8** but using current densities about ten times larger. The current was of 7 μA but the anode was touching the solution only at the tip.

Received: September 7, 2004
Final version: November 3, 2004

[1] a) E. Dagotto, T. M. Rice, *Science* **1996**, *271*, 618. b) D. J. Scalapino, *Nature* **1995**, *377*, 12. c) Z. Hiroi, M. Takano, *Nature* **1995**, *337*, 41. d) M. Azuma, Z. Hiroi, M. Tanako, K. Ishida, I. Kitaoka, *Phys. Rev. Lett.* **1994**, *73,* 3463.

[2] a) D. C. Johnston, J. W. Johnson, D. P. Goshom, A. P. Jacobson, *Phys. Rev. B* **1987**, *35*, 219. b) T. Barnes, J. Riera, *Phys. Rev. B* **1994**, *50*, 6817. c) A. W. Garret, S. E. Nagler, D. A. Tennant, B. C. Sales, T. Barnes, *Phys. Rev. Lett.* **1997**, *79*, 74.

[3] a) T. Matsumoto, Y. Miyazaki, A. S. Albrecht, C. P. Landee, M. M. Turnbull, M. Sorai, *J. Phys. Chem. B* **2000**, *104*, 9993. b) F. M. Woodward, A. S. Albrecht, C. M. Wynn, C. P. Landee, M. M. Turnbull, *Phys. Rev. B.* **2002**, *65,* 144 412. c) B. C. Watson, V. N. Kotov, M. W. Meisel, D. W. Hall, G. E. Granoth, W. T. Montfrooij, S. E. Nagnler, D. A. Jensen, R. Backov, M. A. Petruska, G. E. Fanucci, D. R. Talham, *Phys. Rev. Lett.* **2001**, *86*, 5168. d) G. Chaboussant, M.-H. Julien, Y. Fagot-Revurat, L. P. Lévy, C. Berthier, M. Horvatié, O. Piovesana, *Phys. Rev. Lett.* **1997**, *79*, 925.

[4] a) C. Rovira, J. Veciana, E. Ribera, J. Tarres, E. Canadell, R. Rousseau, M. Mas, E. Molins, M. Almeida, R. T. Henriques, J. Morgado, J.-P. Schoeffel, J.-P. Pouget, *Angew. Chem. Int. Ed. Engl.* **1997**, *36*, 2324. b) C. Rovira, *Chem. Eur. J.* **2000**, *6*, 1723. c) T. Komatsu, N. Kojima, G. Saito, *Solid State Commun.* **1997**, *103*, 519. d) T. Komatsu, N. Kojima, G. Saito, *Synth. Met.* **1999**, *103*, 1923. e) M. Fourmigué, B. Domercq, I. V. Jourdain, P. Molinié, F. Guyon, J. Amaudrut, *Chem. Eur. J.* **1988**, *4*, 1714. f) B. Domercq, C. Coulon, M. Fourmigué, *Inorg. Chem.* **2001**, *40*, 371. g) H. Imai, T. Inabe, T. Otsuka, T. Okumo, K. Awaga, *Phys. Rev. B.* **1996**, *54*, R6338. h) H. Imai, T. Otsuka, T. Naito, K. Awaga, T. Inabe, *J. Am. Chem. Soc.* **1999**, *121*, 8098. i) S. Nishihara, T. Akutagawa, T. Hasegawa, T. Nakamura, *Chem. Commun.* **2002**, 408.

[5] C. Rovira, in *Structure and Bonding* (Ed: J. Veciana), Springer-Verlag, Berlin, Germany **2001**, pp. 163–188.

[6] C. Rovira, J. Veciana, N. Santaló, J. Tarrés, J. Cirujeda, E. Molins, J. Llorca, E. Espinosa, *J. Org. Chem.* **1994**, *59*, 3307.

[7] R. Wesolowski, J. T. Haraldsen, J. L. Musfeldt, T. Barnes, M. Mas-Torrent, C. Rovira, R. T. Henriques, M. Almeida, *Phys. Rev. B* **2003**, *68*, 134 405.

[8] A. Pérez-Benítez, J. Tarrés, E. Ribera, J. Veciana, C. Rovira, *Synthesis* **1999**, *4*, 577.

[9] L.-Y. Chiang, P. Shu, D. Holt, D. O. Cowan, *J. Org. Chem.* **1984**, *49*, 1117.

[10] a) C. K. Johnson, *ORTEP*, Report ORNL-5138, Oak Ridge National Laboratory, Oak Ridge, TN **1976**. b) L. J. Farrugia, *J. Appl. Crystallogr.* **1997**, *30*, 565.

[11] J. B. Torrance, B. W. Scout, F. B. Kaufman, P. E. Seiden, *Phys. Rev. B* **1979**, *19*, 730.

[12] A. Terahara, H. Ohya-Nishigushi, N. Hirota, H. Awaji, T. Kawase, S. Yoneda, T. Sugimoto, Z. Yoshida, *Bull. Chem. Soc. Jpn.* **1984**, *57*, 1760.

[13] C. Rovira, A. Pérez-Benítez, E. Molins, I. Mata, M. Almeida, H. Alves, J. Veciana, V. Gama, E. B. Lopes, R. T. Henriques, *Synth. Met.* **2003**, *133–134*, 523.

[14] J. Tarrés, M. Mas, E. Molins, J. Veciana, C. Rovira, J. Morgado, R. T. Henriques, M. Almeida, *J. Mater. Chem.* **1995**, *5*, 1653.

[15] C. Rovira, S. Le Moustarder, D. Belo, J. Veciana, M. Almeida, V. Gama, M. T. Duarte, *Synth. Met.* **2001**, *120*, 717.

[16] E. B. Lopes, H. Alves, E. Ribera, M. Mas-Torrent, P. Auban-Senzier, E. Canadell, R. T. Henriques, M. Almeida, E. Molins, J. Veciana, C. Rovira, D. Jérome, *Eur. Phys. J. B* **2002**, *29*, 27.

[17] M. Mas-Torrent, H. Alves, E. B. Lopes, M. Almeida, K. Wurst, J. Vidal-Gancedo, J. Veciana, C. Rovira, *J. Solid State Chem.* **2002**, *168*, 563.

[18] a) J. C. Dias, J. Morgado, H. Alves, E. B. Lopes, I. C. Santos, M. T. Duarte, R. T. Henriques, M. Almeida, X. Ribas, C. Rovira, J. Veciana, *Polyhedron* **2003**, *22*, 2447. b) E. B. Lopes, J. C. Dias, J. P. Seiça, I. C. Santos, J. Morgado, R. T. Henriques, M. Almeida, X. Ribas, K. Wurst, J. Veciana, C. Rovira, P. Foury-Leylekian, *J. Phys. IV* **2004**, *114*, 537.

[19] X. Ribas, M. Mas-Torrent, C. Rovira, J. Veciana, J. C. Dias, H. Alves, E. B. Lopes, M. Almeida, K. Wurst, *Polyhedron* **2003**, *22*, 2415.

[20] B. G. Werden, E. Billig, H. B. Gray, *Inorg. Chem.* **1966**, *5*, 78.

[21] M. J. Matos, R. T. Henriques, L. Alcácer, in *Lower-Dimensional Systems and Molecular Electronics* (Eds: R. M. Metzger, P. Day, G. Papavassiliou), Plenum Press, New York **1989**.

[22] M. J. Matos, I. C. Santos, R. T. Henriques, M. T. Duarte, *Synth. Met.* **1991**, *41–43*, 2155.

[23] Cyclic voltammetry experiments on (*n*-Bu_4N)$_2$[Au(i-mnt)$_2$] complex indicates its decomposition at potentials above 0.5 V. It has been determined by addition of I_2 at –78 °C that the decomposition products after oxidation yields the dimeric Au(I) species [Au^I_2(i-mnt)$_2$]$^{2-}$, due to the formation of green intermediates assigned to [Au^{II}_2(i-mnt)$_2$-$(I)_2$]$^{2-}$. Further details on the redox chemistry of these gold species

ADVANCED FUNCTIONAL MATERIALS

are found in: a) N. I. Khan, J. P. Fackler, Jr., C. King, J. C. Wang, S. Wang, *Inorg. Chem*. **1988**, *27*, 1672. b) N. I. Khan, S. Wang, J. P. Fackler, Jr., *Inorg. Chem*. **1989**, *28*, 3579.

[24] A. Maspero, I. Kani, A. A. Mohamed, M. A. Omary, R. J. Staples, J. P. Fackler, Jr., *Inorg. Chem.,* **2003**, *42*, 5311.

[25] E. Coronado, C. J. Gómez-Garcia, *Chem. Rev*. **1998**, *98*, 273.

[26] M. Troyer, D. Tsunetsugu, D. Würtz, *Phys. Rev. B* **1994**, *50*, 13 315.

[27] M. Troyer, E. Zhitomirsky, K. Ueda, *Phys. Rev. B* **1997**, *55*, 6117.

[28] a) V. Gama, M. Almeida, R. T. Henriques, I. C. Santos, A. Domingos, S. Ravy, J. P. Pouget, *J. Phys. Chem*. **1991**, *95*, 4263. b) V. Gama, R. T. Henriques, M. Almeida, J. P. Pouget, *Synth. Met.* **1993**, *55–57*, 1677. c) V. Gama, R. T. Henriques, M. Almeida, L. Alcácer, *J. Phys. Chem.* **1994**, *98*, 997.

[29] M. Almeida, R. T. Henriques, in *Organic Conductive Molecules and Polymers* (Ed.: H. S. Nalwa), John Wiley and Sons, Chichester, UK **1997**, pp. 87–149.

[30] J. D. Forrester, A. Zalkin, D. H. Templeton, *Inorg. Chem.* **1964**, *3*, 1500.

[31] E. Ribera, C. Rovira, J. Veciana, J. Tarrés, E. Canadell, R. Rousseau, E. Molins, M. Mas, J.-P. Schoeffel, J.-P. Pouget, J. Morgado, R. T. Henriques, M. Almeida, *Chem. Eur. J.* **1999**, *5*, 2025.

[32] J. C. Dias, E. B. Lopes, I. C. Santos, M. T. Duarte, R. T. Henriques, M. Almeida, X. Ribas, C. Rovira, J. Veciana, P. Foury-Leylekian, J.-P. Pouget, P. Auban-Senzier, D. Jérome, *J. Phys. IV* **2004**, *114*, 497.

[33] a) A. Davison, N. Edelstein, R. H. Holm, A. H. Maki, *Inorg. Chem.* **1963**, *2*, 1227. b) A. Davison, R. H. Holm, *Inorg. Synth*. **1967**, *10*, 8.

[34] L. Persaud, C. Langford, *Inorg. Chem.* **1985**, *24*, 3562.

[35] C. K. Fair, *MolEN, An Interactive Intelligent System for Crystal Structure Analysis*, Delft, The Netherlands **1990**.

[36] G. M. Sheldrick, *Acta Crystallogr. A* **1990**, *46*, 467.

[37] SIR97—A. Altomare, M. C. Burla, M. Camalli, G. L. Cascarano, C. Giacovazzo, A. Guagliardi, A. G. G. Moliterni, G. Polidori, R. Spagna, *J. Appl. Crystallogr.* **1999**, *32*, 115–119.

[38] G. M. Sheldrick, University of Göttingen: Göttingen, Germany **1997**. SHELX97—Programs for Crystal Structure Analysis (Release 97-2). G. M. Sheldrick, Institüt für Anorganische Chemie der Universität, Tammanstrasse 4, D-3400 Göttingen, Germany **1998**.

[39] M. Almeida, S. Oostra, L. Alcácer, *Phys. Rev. B* **1984**, *30*, 2839.

[40] E. B. Lopes, INETI-Sacavém, internal report, Sacavem, Portugal **1991**.

[41] R. P. Huebner, *Phys. Rev. A* **1964**, *135*, 1281.

[42] P. E. Schafer, F. Wudl, G. A. Thomas, J. P. Ferraris, D. O. Cowan, *Solid State Commun*. **1974**, *14*, 347.

